Hydrogeology Journal (2020) 28:2259–2274
https://doi.org/10.1007/s10040-020-02175-1

PAPER

Generalized hydraulic conductivity model for capillary and adsorbed film flow

Ke Chen[1] · He Chen[1]

Received: 22 October 2019 / Accepted: 26 April 2020 / Published online: 13 June 2020

Abstract

Commonly used transport models of unsaturated flow assume that the movement of pore water is dominated mainly by capillary flow and they neglect adsorbed film flow. These models have been proven to be successful at high and intermediate saturations but typically underestimate the hydraulic conductivity in the dry range, where water movement in equilibrium conditions is dominated by adsorbed film flow. Given these considerations, this paper proposes a simplified configuration of pore water that accounts for the transport processes of both capillary and film flow. Based on the mechanisms of soil water retention, a conception of the specific thickness of the adsorbed film is defined to describe the adsorption strength and adsorption capacity of porous media. Furthermore, a statistical physically based model of relative hydraulic conductivity in the full range of suction is derived. Fractal and Monte Carlo methods are used to determine the pore size distribution of porous media and then the corresponding specific model of relative hydraulic conductivity is derived. The results show that the proposed model agrees well with the experimental data in the entire suction range. It is also found that the pore size distribution of porous media controls the transport characteristic of capillary water but not adsorption film flow which is only related to the mineral content, mineral species, and specific surface area. Additionally, the influences of the model parameters on the transport of porous media are also addressed.

Keywords Hydraulic properties · Adsorbed film flow · Matric suction · Fractal · Numerical modeling

Introduction

Estimating the hydraulic conductivity of unsaturated porous media is fundamental to the accurate modeling of hydrological processes such as seepage, evaporation and solute transport in porous media (Durner and Fluhler 2005; Šimůnek 2005; Collis-George 2010). Measurement of the hydraulic conductivity of an unsaturated porous medium is very time consuming and difficult, especially at a low value of saturation. As an alternative to direct measurement, models have been extensively and intensively studied to estimate the hydraulic conductivity of unsaturated porous media (Burdine 1953; Brooks and Corey 1964; Mualem 1976; van Genuchten 1980; Alexander and Skaggs 1986; Kosugi 1996; Guarracino et al. 2014).

✉ He Chen
hchen@hnu.edu.cn

Ke Chen
kechen0216@hnu.edu.cn

[1] Department of Geotechnical Engineering, Tongji University, Shanghai 200092, China

Accurately predicting the hydraulic conductivity of porous media over the entire range of matric heads remains a persistent challenge. This may be due to the complexity of the pore structure network and the different water retention mechanisms of soil in the dry and wet ranges. So-called capillary-dependent models such as the Mualem model (Mualem 1976) and the Burdine model (Burdine 1953), have received great attention and are well suited for many specific situations. These models conceptualize pore spaces as tortuous cylindrical tubes occupied by either wet or nonwet phases. In general, they can successfully predict hydraulic conductivity at high to intermediate saturation, where water is primarily retained by capillary forces. However, in the dry or very dry region, these models underestimate the hydraulic conductivity of unsaturated porous media, which has been indicated in many experiments and theoretical studies (Lenormand; 1990; Toledo et al. 1990; Goss and Madliger 2007; Jansik 2009).

Driven by these limitations, the adsorption surface force has been taken into account in recent years to expand the capillary models (Tuller et al. 1999; Tuller and Or 2001; Peters and Durner 2008; Tokunaga 2009; Lebeau and Konrad 2010; Peters 2013; Zhang 2011; Rudiyanto et al.

2015). Based on thermodynamic considerations, Tuller and Or (2001) proposed a specific angular pore space that takes into account capillary flow, corner flow, and film flow to derive a hydraulic conductivity model in the full matric head range. Despite its scientific success, the application of this model has been limited because of the mathematical complexity and the use of specific pore size distributions. Peters and Durner (2008) applied Mualem's capillary model and an empirical power function to describe the hydraulic conductivity of capillary flow and adsorption film flow, respectively. Their models fit well with experimental data, but there is no theoretical basis for the hydraulic conductivity function of the film flow. The subsequent key contribution to estimating the hydraulic conductivity within both wet and dry regions is by Lebeau and Konrad (2010). They suggested that the capillary flow process satisfies the Young-Laplace equation, while the adsorbed water stretches over the surface of the soil particles to form a continuous thin film and flows in the form of annuli. In their model, capillary hydraulic conductivity is again proposed by a capillary bundle function, whereas the thin film hydraulic conductivity is described by a more complicated hydrodynamic function.

Film flow is usually considered to be planar adsorption described by disjoining pressure, which only involves the adsorption strength of soils without describing the adsorption capacity related to the specific surface area of soils and hydrophilic minerals. In this study, a new physical concept of specific thickness is defined to describe the adsorption strength and adsorption capacity of soils. Furthermore, a physically based statistical model of relative hydraulic conductivity in the full range of the matric head is derived. For the application of the model, a fractal scaling law is also included in this study to obtain a continuous analytic expression. The model performance is subsequently appraised by published data sets from sand to loam.

Mechanisms for water retention

From a fundamental physics perspective, the retention mechanism of soil water involves two concepts: capillarity and adsorption. These two water retention mechanisms act on different stages of soil water content, which correspond to different suction ranges and generally have no direct interdependencies.

Capillarity refers to the interaction of three components: pore air, pore water, and soil particles. Using capillary force to describe the suction of wet to moderately wet unsaturated soil is successful because the suction in this range (most likely less than 400 kPa) can be well determined by the equilibrium of air pressure, pore-water pressure, contact angle, and water surface tension (Lu 2016). The physical mechanism of capillarity can be expressed by the Young-Laplace equation as

$$h = \frac{C}{r} \tag{1}$$

where h is the matric head and r is the radius of a pore. $C=2\sigma\cos\theta/\rho g$, where σ is the water surface tension, θ is the contact angle which is assumed to be a constant in this paper, g is the gravity acceleration constant, and ρ is the density of bulk pore water.

In addition, from the Young-Laplace equation, it is clear that pore water retained by capillarity favors small pores with a given matric head/suction. In this case, for unsaturated porous media, it is assumed that there exists a critical value r_c that controls whether the pores are completely filled with capillary water. In other words, all pores with radius $r \leq r_c$ are filled by bulk water (see state II of Fig. 1).

For very dry soils (see state III of Fig. 1), the retention mechanism of soil water involves adsorption corresponding to low matric potential or high suction (Lu 2016). At this time, the concept of soil suction defined by the pressure difference

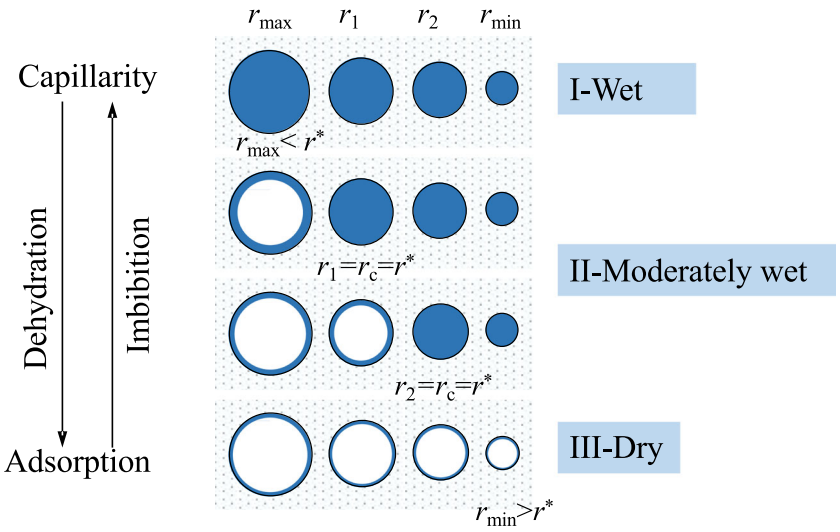

Fig. 1 Illustration of liquid configuration in each stage for capillarity and adsorption. Stage (I): In the wet stage, all of the pores are completely saturated; Stage (II): in the moderately wet stage, the pores with radius $r<r_c$ are liquid saturated and the surfaces of other pores are covered by adsorbed film; Stage(III): in the dry stage, the surface of each pore is covered by adsorbed film. (Note that r_{max}, r_1, r_2, r_{min} are the pore size; r_c is the critically filled radius of pores; r^* is the suction characteristic radius)

between air and pore water may be incomplete. In general, adsorption can be summarized as the process by which water vapor molecules move to soil particles or liquid surfaces. The process ceases when the interaction between air pressure and the adsorbed layer reaches thermodynamic equilibrium. Therefore, general soil suction, from a thermodynamic perspective, should be determined by the energy difference between matric potential and air pressure (Khorshidi and Lu 2017).

From the viewpoint of energy, the concept of disjoining pressure Π of a planar film can well describe the matric suction or potential of the adsorption layer (Lu and Zhang 2019). Disjoining pressure derives from overlapping double ionic layers, boundary electromagnetic fluctuation fields, and boundary layers of liquids (Derjaguin and Churaev 1974). Therefore, in porous media, disjoining pressure is generally considered to have three different components, ionic-electrostatic Π_e, molecular Π_m, and structure Π_s. However, the first two components are commonly considered when studying the adsorption layer.

Ionic-electrostatic adsorption is primarily due to the osmosis produced by the difference in ion concentration between the substrate surface and the solution, which forces the ions of the substrate to diffuse out of the surface to reach equilibrium with the concentrations of the ions in the solution. For the case of a low concentration of symmetrical electrolyte with a high potential substrate, Langmuir (1938) solved the Poisson-Boltzmann equation to obtain the disjoining pressure of ionic-electrostatic components:

$$\Pi_e(\omega) = \frac{\varepsilon_0 \varepsilon}{2}\left(\frac{\pi k_B T}{eZ}\right)^2 \frac{1}{\omega^2} \tag{2}$$

where ω is the film thickness, ε_0 is the permittivity of free space, ε is the relative permittivity of water, k_B is the Boltzmann constant, T is the Kelvin temperature, Z is the ion change, and e is the electron charge.

Molecular adsorption dominated by van der Waals forces can produce particle surface hydration and multilayer adsorption (Derjaguin et al. 1987; Israelachvili 2011; Lu 2016; Lu and Zhang 2019; Zhang and Lu 2018). A continuous movable water film retained by van der Waals forces on soil particle surfaces can produce suction up to a few hundreds of MPa. The molecular component of disjoining pressure contributed by van der Waals interactions for a planar film can be expressed as (Derjaguin et al. 1987)

$$\Pi_m(\omega) = -\frac{A_H}{6\pi\omega^3} \tag{3}$$

where A_H is the Hamaker constant. Note that Eqs. (2) and (3) are derived on the assumption that the surface of the material is smooth.

The adsorption mechanism of water vapor molecules described by disjoining pressure is mainly directed to planar adsorption. Equations (2) and (3) study the relationship between adsorption strength and material properties but cannot explain the adsorption capacity of granular porous media, which is related to the specific surface area and hydrophilic minerals. Therefore, it is necessary to define the amount of adsorption per unit volume $\overline{\theta}$ (at a given suction, adsorbed water film volume of a grain divided by the grain volume). Since the thickness of the adsorption layer is small (nanometer to micrometer), the amount of adsorption per unit volume can be written as

$$\overline{\theta} = \frac{\theta_a}{V} = \frac{\omega S}{V} = \omega S_{specific} \tag{4}$$

where θ_a is the adsorbed water film volume of a grain, V is the grain volume, S is the surface area of the grain, and $S_{specific}$ is the specific surface area. The specific surface area can be expressed as follows:

$$S_{specific} = \lambda \cdot \frac{1}{r} \tag{5}$$

where λ is the shape factor (e.g., for spherical grains, λ=3; for cylindrical pores, λ=2), and r is the radius of grains or pores.

Substituting Eq. (5) into Eq. (4) yields

$$\overline{\theta} = \lambda \cdot \frac{\omega}{r} = \lambda \cdot \delta \tag{6}$$

where $\delta = \omega/r$ is defined as the specific thickness of adsorbed water. From the definition of the specific thickness, δ can not only describe the adsorption strength of a material but also explain the relationship between the adsorption capacity and the particle (pore) size. Figure 2 shows a conceptual diagram of the configuration and specific thickness of the adsorbed film in a cylindrical pore.

Although the Young-Laplace equation is inadaptable to the case of adsorbed water film, for any given matric potential/suction/head, it can still find a corresponding value defined as suction characteristic radius r^* (see Fig. 1), that is, $h=\Pi(\omega)/\rho g = C/r^*$. Therefore, combined with Eqs. (2) and (3), the relationship between the thickness ω of the adsorbed film and the suction characteristic radius r^* can be expressed as

$$\ln\omega \propto \ln r^* \tag{7}$$

Furthermore, the following relationship is also assumed to be satisfied:

$$\ln\delta = \ln\frac{\omega}{r} \propto \ln\frac{r^*}{r} \tag{8}$$

Consequently, the specific thickness of the adsorbed film can be described by the suction characteristic radius r^* and the pore (particle) radius r as

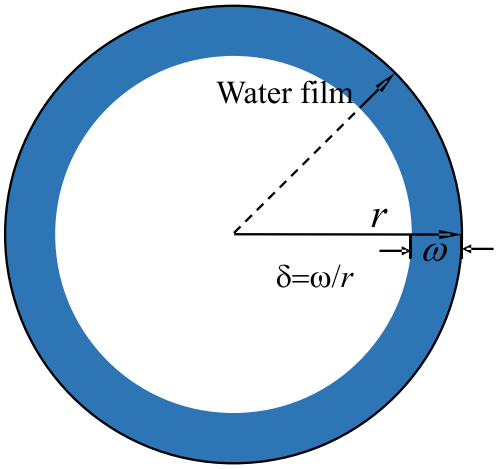

Fig. 2 A conceptual diagram of the configuration and specific thickness of the adsorbed film in a cylindrical pore

$$\delta = \beta\left(\frac{r^*}{r}\right)^{\alpha} \tag{9}$$

where α and β are the model parameters related to adsorption strength and adsorption capacity of materials, respectively. More specifically, α is controlled by the type of soil minerals. The higher valence of soil mineral ions means stronger adsorption strength, which corresponds to a larger α. A larger β means that the soil has greater adsorption capacity, corresponding to a larger specific surface area and more hydrophilic mineral components. The characteristics of these parameters will be discussed further in section 'Model features and parameters determination'. Figure 3 shows the δ–r^*–r three-dimensional (3D) surface map with α=0.3 and β=0.03.

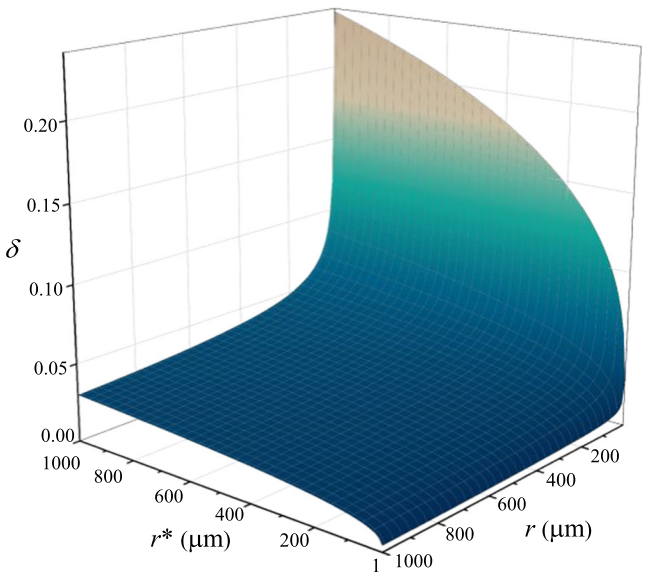

Fig. 3 Specific thickness surface determined by pore (particle) size and suction characteristic radius

Statistical scale analysis for hydraulic conductivity

Roughness and irregularity of pores make it difficult to accurately simulate the hydraulic properties of porous media. In this study, to simplify the model, the pores are reduced to a cluster of tortuous capillary tubes with smooth inner surfaces (see Fig. 1). According to the mechanisms of water retention in the preceding description, liquid flow in the moderately wet range may occur through all smaller pores that are filled by bulk water as well as through the larger pores covered by continuous film flow (see state II of Fig. 1). In the dry range, liquid flow only occurs through the film flow absorbed on the surface of pores (see state III of Fig. 1). Therefore, for unsaturated porous media, the transport process of the bulk water can be divided into two stages: both capillary flow and film flow participate in water transport (water retention dominated by capillarity, corresponding to a moderate matric head range) and water transport only contributed by film flow (water retention dominated by adsorption, corresponding to a high matric head range). To evaluate the transport characteristics of unsaturated flow, it is necessary to determine the hydraulic conductivity in the saturated state.

For saturated porous media (see state I of Fig. 1), pore water movement can generally be considered Poiseuille flow. Therefore, the volumetric flow rate of an individual tortuous pore can be determined by the Hagen-Poiseuille equation (Bousfield and Karles 2004):

$$q_{\mathrm{p}}(r) = \frac{\pi r^4}{8\mu}\frac{\Delta P}{\tau L_0} \tag{10}$$

where μ is the viscosity of bulk water, L_0 is the representative length of a pore, and ΔP is the pressure drop. τ is the pore tortuosity, and $\tau = L_{\mathrm{t}}/L_0$, where L_{t} is the tortuous length of the pore. For a representative elementary volume (REV) with a pore radius varying from $r_{\min}$ to $r_{\max}$ (see Fig. 1), the total flow rate can be captured by accumulating the volumetric flow rate of each pore:

$$Q_{\mathrm{S,t}} = \frac{\pi}{8\mu}\frac{\Delta P}{L_0}\sum_{i=1(r_{\min})}^{n(r_{\max})}\frac{r_i^4}{\tau_i} \tag{11}$$

where r_i is the radius of the ith pore and τ_i is the corresponding pore tortuosity.

On the other hand, based on Darcy's law, the total volume flow rate of the REV can also be specified as

$$Q_{\mathrm{S,t}} = K_{\mathrm{s}}\frac{\Delta P}{L_0}A_{\mathrm{REV}} \tag{12}$$

where K_{s} is the hydraulic conductivity in the saturated state and A_{REV} is the cross-section area of the REV.

Hence, substituting Eq. (11) into the rearranged Eq. (12) yields

$$K_s = \frac{\pi}{8\mu A_{REV}} \sum_{i=1(r_{min})}^{n(r_{max})} \frac{r_i^4}{\tau_i} \tag{13}$$

Equation (13) is a statistical scale analysis used to determine the hydraulic conductivity in the saturated state, which is the benchmark for evaluating the relative hydraulic conductivity of unsaturated REV.

Water movement of moderately wet range in porous media

As shown in Fig. 1, in the moderately wet range, the liquid flow may occur through all smaller pores filled by the bulk water as well as through the larger pores covered by continuous film flow. Under the assumption of ignoring the coupling behavior of capillary and adsorbed water-transport in porous media, the total flow rate can be expressed as

$$Q_{U,t} = Q_{U,t}^C + Q_{U,t}^F \tag{14}$$

where $Q_{U,t}^C$ and $Q_{U,t}^F$ are the volumetric flow rates of capillary flow and film flow, respectively.

For the capillary flow, the volumetric flow rate $Q_{U,t}^C$ can also be captured by accumulating the pore flow rate described by Eq. (10) with a radius from r_{min} to r_c, that is,

$$Q_{U,t}^C(r_c) = \frac{\pi}{8\mu}\frac{\Delta P}{L_0} \sum_{i=1(r_{min})}^{j(r_c)} \frac{r_i^4}{\tau_i} \tag{15}$$

Considering the hydrodynamic behavior of annular film flow, the volumetric flow rate q^F of film flow in a single pore can be described as

$$q^F(\omega) = \bar{v}_p(\omega) A_F \tag{16}$$

where $\bar{v}_p(\omega)$ is the average liquid velocity with a given film thickness ω, and A_F is the cross-section area of the film flow. In the case of the flow velocity distribution normal to the cross-section of the film, the simplified Navier-Stokes equation can be solved to obtain the average flow velocity $\bar{v}_p(\omega)$ (Or and Tuller 2000):

$$\bar{v}_p(\omega) = \frac{\omega^2}{3\mu}\frac{\Delta P}{\tau L_0} \tag{17}$$

Note that for simplicity, only thick films are considered here (more than tens of layers of water molecules) because for very thin films (several layers of water molecules), liquid viscosity is likely to be elevated relative to bulk water due to long- and short-range interfacial forces (McBride and Baveye 1995).

For annular film flow (see Fig. 2), the cross-section area A_F can be determined by the specific thickness δ:

$$A_F = \left[1-(1-\delta)^2\right]\pi r^2 \tag{18}$$

Combined with Eqs. (9), (16), (17), and (18), the flow rate $Q_{U,t}^F$ of film can be specified as

$$Q_{U,t}^F(r_c) = \frac{\pi}{3\mu}\frac{\Delta P}{L_0} \times \sum_{i=j(r_c)}^{n(r_{max})} \left(2\beta^3 {r_c}^{3\alpha}\frac{r_i^{4-3\alpha}}{\tau_i} - \beta^4 {r_c}^{4\alpha}\frac{r_i^{4-4\alpha}}{\tau_i}\right) \tag{19}$$

It should be noted that in a moderately wet range, the suction can be determined by the Young-Laplace equation. Hence, the suction characteristic radius r^* can be replaced with the critical radius r_c in Eq. (19).

Therefore, the total flow rate $Q_{U,t}$ is

$$Q_{U,t} = \frac{\pi}{8\mu}\frac{\Delta P}{L_0}\sum_{i=1(r_{min})}^{j(r_c)}\frac{r_i^4}{\tau_i} + \frac{\pi}{3\mu}\frac{\Delta P}{L_0} \times \sum_{i=j(r_c)}^{n(r_{max})} \left(2\beta^3 {r_c}^{3\alpha}\frac{r_i^{4-3\alpha}}{\tau_i} - \beta^4 {r_c}^{4\alpha}\frac{r_i^{4-4\alpha}}{\tau_i}\right) \tag{20}$$

On the other hand, Buckingham–Darcy's law (Buckingham 1907) describes the transport law of unsaturated flow involving the total flow rate:

$$Q_{U,t} = K_s k_r \frac{\Delta P}{L_0} A_{REV} \tag{21}$$

where k_r is the relative hydraulic conductivity, K_s is the hydraulic conductivity of the saturated REV, and A_{REV} is the cross-section area of the REV.

Consequently, the expression of relative hydraulic conductivity is obtained by substituting Eq. (20) into the rearranged Eq. (21) and combining Eq. (13):

$$k_r(r_c) = \sum_{i=1(r_{min})}^{j(r_c)}\frac{r_i^4}{\tau_i} \Big/ \sum_{i=1(r_{min})}^{n(r_{max})}\frac{r_i^4}{\tau_i} + \frac{8}{3} \times \sum_{i=j(r_c)}^{n(r_{max})} \left(2\beta^3 {r_c}^{3\alpha}\frac{r_i^{4-3\alpha}}{\tau_i} - \beta^4 {r_c}^{4\alpha}\frac{r_i^{4-4\alpha}}{\tau_i}\right) \Big/ \sum_{i=1(r_{min})}^{n(r_{max})}\frac{r_i^4}{\tau_i} \tag{22}$$

where the first and second terms on the right side are the relative hydraulic conductivity of capillary flow and adsorbed film flow, respectively.

Water movement of dry range in porous media

In the high suction range (above 1,000 kPa), water movement may only occur through the pores (or grains) that are covered by films. In this case, water retention is dominated by ionic-electrostatic and molecular forces. Similarly, the total flow rate of film flow can be obtained by accumulating the flow rate of each pore:

$$Q_{\mathrm{U,t}}(r^*) = \frac{\pi}{3\mu}\frac{\Delta P}{L_0} \times \sum_{i=1(r_{\min})}^{n(r_{\max})}\left[2\beta^3(r^*)^{3\alpha}\frac{{r_i}^{4-3\alpha}}{\tau_i} - \beta^4(r^*)^{4\alpha}\frac{{r_i}^{4-4\alpha}}{\tau_i}\right] \quad (23)$$

Further, substituting Eqs. (13) and (23) into the rearranged Eq. (21) yields a relative hydraulic conductivity for a given suction characteristic radius r^*:

$$k_{\mathrm{r}}(r^*) = \frac{8}{3}\sum_{i=1(r_{\min})}^{n(r_{\max})}\left[2\beta^3(r^*)^{3\alpha}\frac{{r_i}^{4-3\alpha}}{\tau_i} - \beta^4(r^*)^{4\alpha}\frac{{r_i}^{4-4\alpha}}{\tau_i}\right] \Big/ \sum_{i=1(r_{\min})}^{n(r_{\max})}\frac{{r_i}^4}{\tau_i} \quad (24)$$

In summary, in the full suction range, the transport law of porous media can be described by

$$k_{\mathrm{r}} = \begin{cases} \left[\sum_{i=1(r_{\min})}^{j(r_{\mathrm{c}})}\frac{{r_i}^4}{\tau_i} + \frac{8}{3}\sum_{i=j(r_{\mathrm{c}})}^{n(r_{\max})}\left(2\beta^3{r_{\mathrm{c}}}^{3\alpha}\frac{{r_i}^{4-3\alpha}}{\tau_i} - \beta^4{r_{\mathrm{c}}}^{4\alpha}\frac{{r_i}^{4-4\alpha}}{\tau_i}\right)\right] \Big/ \sum_{i=1(r_{\min})}^{n(r_{\max})}\frac{{r_i}^4}{\tau_i} & ,\ r^*(=r_{\mathrm{c}}) \geq r_{\min} \\ \frac{8}{3}\sum_{i=1(r_{\min})}^{n(r_{\max})}\left[2\beta^3(r^*)^{3\alpha}\frac{{r_i}^{4-3\alpha}}{\tau_i} - \beta^4(r^*)^{4\alpha}\frac{{r_i}^{4-4\alpha}}{\tau_i}\right] \Big/ \sum_{i=1(r_{\min})}^{n(r_{\max})}\frac{{r_i}^4}{\tau_i} & ,\ r^* < r_{\min} \end{cases} \quad (25)$$

Equation (25) is a generalized statistical model for the hydraulic conductivity of unsaturated flows, which involves pore size distribution, pore tortuosity, adsorption strength and adsorption capacity of porous media. However, Eq. (25) cannot be directly used to predict the relative hydraulic conductivity of unsaturated porous media; therefore, the pore size distribution (PSD) function needs to be determined.

Specific model of relative hydraulic conductivity

In the previous section, a generalized statistical model was proposed to simulate the transport of capillary and adsorbed water in unsaturated porous media. For the application of the generalized statistical model, it is necessary to define the PSD function.

Many PSD functions have been applied in the literature to construct soil pore systems, including Gaussian distribution (Xu and Torres-Verdín 2013), lognormal distribution (Kosugi 1994), gamma distribution (Tuller and Or 2001), and fractal scale law (Yu and Cheng 2002). Any of these functions can be used with the generalized statistical model. In this study, the fractal scaling law of PSD is employed as an example to derive the specific model of relative hydraulic conductivity.

Since assuming that the pore size of porous media has statistically self-similar fractal scaling laws, the cumulative number of pores whose size is larger than a measured scale r can be expressed as (Yu and Cheng 2002)

$$N(\varepsilon \geq r) = \left(\frac{r}{r_{\max}}\right)^{-D_{\mathrm{f}}} \quad (26)$$

where D_{f} is the area fractal dimension with a range of 1–2. Then, the number of pores in an infinitesimal range r to r+dr can be obtained by differentiating Eq. (26) as

$$\mathrm{d}N(r) = -D_{\mathrm{f}}{r_{\max}}^{D_{\mathrm{f}}}r^{-D_{\mathrm{f}}-1}\mathrm{d}r \quad (27)$$

where the negative sign (−) denotes that the pore number decreases with increasing size. In fact, Eq. (27) quantifies the number of pores at a given pore size. Therefore, substituting Eq. (27) into Eq. (22) yields

$$k_{\mathrm{r}}(r_{\mathrm{c}}) = \left[\int_{r_{\min}}^{r_{\mathrm{c}}}\frac{D_{\mathrm{f}}{r_{\max}}^{D_{\mathrm{f}}}}{\tau(r)}r^{3-D}\mathrm{d}r + \frac{8}{3}D_{\mathrm{f}}{r_{\max}}^{D_{\mathrm{f}}}\int_{r_{\mathrm{c}}}^{r_{\max}}\left(\frac{2\beta^3{r_{\mathrm{c}}}^{3\alpha}r^{3-3\alpha-D_{\mathrm{f}}}}{\tau(r)} - \frac{\beta^4{r_{\mathrm{c}}}^{4\alpha}r^{3-4\alpha-D_{\mathrm{f}}}}{\tau(r)}\right)\mathrm{d}r\right] \Big/ \int_{r_{\min}}^{r_{\max}}\frac{D_{\mathrm{f}}{r_{\max}}^{D_{\mathrm{f}}}r^{3-D_{\mathrm{f}}}}{\tau(r)}\mathrm{d}r \quad (28)$$

Table 1 Soils Used in This Study and Their Measured Properties

Data Set	Reference	Porosity, n	K_s (m/s)
Sandy loam	Pachepsky et al. (1984)	0.43	9.26×10^{-7}
Silt loam	Pachepsky et al. (1984)	0.53	3.55×10^{-7}
Clay loam	Pachepsky et al. (1984)	0.50	5.79×10^{-8}
Pachapa fine sandy clay	Mualem (1976b)	0.33	1.40×10^{-6}
Gilat loam	Mualem (1976b)	0.44	2.00×10^{-6}
Poederlee loamy sand	Nemes et al. (2001)	0.42	2.79×10^{-5}
Peoderlee sand	Nemes et al. (2001)	0.42	1.90×10^{-5}
Cubbaroo clay loam	Minasny and Field (2005)	–	–
Fine Sand	Minasny and Field (2005)	–	–
Berlin Sand	Peters (2013)	–	–

Additionally, the tortuosity τ can be determined by the tortuosity fractal scaling law (Yu and Cheng 2002):

$$\tau = \left(\frac{L_0}{2r}\right)^{D_T-1} \tag{29}$$

where D_T is the tortuosity fractal dimension with a range of 1–2, which describes the convoluted extent of pore channels for fluid flow in porous media. Note that D_T=1 implies a straight pore channel and D_T=2 represents an infinitely tortuous line. In addition, substituting Eq. (29) into Eq. (28) yields

$$k_r(r_c) = \frac{{r_c}^{C_f} - r_{min}^{C_f}}{r_{max}^{C_f} - r_{min}^{C_f}} + \frac{16\beta^3}{3}\frac{C_f}{C_f-3\alpha}\frac{{r_c}^{3\alpha} r_{max}^{C_f-3\alpha} - {r_c}^{C_f}}{r_{max}^{C_f} - r_{min}^{C_f}} - \frac{8\beta^4}{3}\frac{C_f}{C_f-4\alpha}\frac{{r_c}^{4\alpha} r_{max}^{C_f-4\alpha} - {r_c}^{C_f}}{r_{max}^{C_f} - r_{min}^{C_f}} \tag{30}$$

where C_f=3–D_f+D_T is the fractal factor that is subject to 2<C_f<4.

Similarly, for the case of high suction (see state III of Fig. 1), the relative hydraulic conductivity can be written as

$$k_r(r^*) = \frac{16\beta^3}{3}\frac{C_f}{C_f-3\alpha}\frac{(r^*)^{3\alpha}\left(r_{max}^{C_f-3\alpha} - r_{min}^{C_f-3\alpha}\right)}{r_{max}^{C_f} - r_{min}^{C_f}} - \frac{8\beta^4}{3}\frac{C_f}{C_f-4\alpha}\frac{(r^*)^{4\alpha}\left(r_{max}^{C_f-4\alpha} - r_{min}^{C_f-4\alpha}\right)}{r_{max}^{C_f} - r_{min}^{C_f}} \tag{31}$$

Therefore, based on the fractal scaling law, the relative hydraulic conductivity of full-range suction can be expressed as

$$k_r = \begin{cases} \dfrac{{r_c}^{C_f} - r_{min}^{C_f}}{r_{max}^{C_f} - r_{min}^{C_f}} + \dfrac{16\beta^3}{3}\dfrac{C_f}{C_f-3\alpha}\dfrac{{r_c}^{3\alpha} r_{max}^{C_f-3\alpha} - {r_c}^{C_f}}{r_{max}^{C_f} - r_{min}^{C_f}} - \dfrac{8\beta^4}{3}\dfrac{C_f}{C_f-4\alpha}\dfrac{{r_c}^{4\alpha} r_{max}^{C_f-4\alpha} - {r_c}^{C_f}}{r_{max}^{C_f} - r_{min}^{C_f}} & , r^*(=r_c) \geq r_{min} \\ \dfrac{16\beta^3}{3}\dfrac{C_f}{C_f-3\alpha}\dfrac{(r^*)^{3\alpha}\left(r_{max}^{C_f-3\alpha} - r_{min}^{C_f-3\alpha}\right)}{r_{max}^{C_f} - r_{min}^{C_f}} - \dfrac{8\beta^4}{3}\dfrac{C_f}{C_f-4\alpha}\dfrac{(r^*)^{4\alpha}\left(r_{max}^{C_f-4\alpha} - r_{min}^{C_f-4\alpha}\right)}{r_{max}^{C_f} - r_{min}^{C_f}} & , r^* < r_{min} \end{cases} \tag{32}$$

On the other hand, the critical radius r_c or the suction characteristic radius r^* can be replaced by matric head h to obtain a k_r–h analytical solution for unsaturated porous media:

$$k_r = \begin{cases} \left(\dfrac{h}{h_{c,min}}\right)^{-C_f} + \dfrac{16\beta^3}{3}\dfrac{C_f}{C_f-3\alpha}\left[\left(\dfrac{h}{h_{c,min}}\right)^{-3\alpha} - \left(\dfrac{h}{h_{c,min}}\right)^{-C_f}\right] - \dfrac{8\beta^4}{3}\dfrac{C_f}{C_f-4\alpha}\left[\left(\dfrac{h}{h_{c,min}}\right)^{-4\alpha} - \left(\dfrac{h}{h_{c,min}}\right)^{-C_f}\right] & , h \leq h_{c,max} \\ \dfrac{16\beta^3}{3}\dfrac{C_f}{C_f-3\alpha}\left(\dfrac{h}{h_{c,min}}\right)^{-3\alpha} - \dfrac{8\beta^4}{3}\dfrac{C_f}{C_f-4\alpha}\left(\dfrac{h}{h_{c,min}}\right)^{-4\alpha} & , h > h_{c,max} \end{cases} \tag{33}$$

where $h_{c,max}$ and $h_{c,min}$ are the maximum and minimum matric head retained by capillarity, respectively. α ($0<\alpha<1$) is the adsorption strength, and β ($0<\beta<1$) represents the adsorption capacity of the materials. Note that since $h_{c,min}/h_{c,max}<<10^{-2}$, $(h_{c,max}/h_{c,min})^{-Cf}=0$ has been introduced in Eq. (33) to simplify the proposed fractal model.

It is interesting to compare the proposed model in the high matric head range with the method by Peters (2013). Peters' film hydraulic conductivity is empirically described by a power function, $k_r^{film}(h) = w(h/h_a)^{-\xi}$, where w and ξ are the fitting parameters, h_a is the air entry value similar to $h_{c,min}$ in this study. The power function is indeed similar to the proposed model within the film-dominated range (i.e., $h>h_{c,max}$) if $16\beta^3 C_f/3(C_f-3\alpha)=w$ and $3\alpha=\xi$.

Model analysis and evaluation

Data sets

Ten published data sets were selected to analyze and evaluate the proposed model. The data sets comprised silt loam, Sandy Loam, and clay loam (Pachepsky et al. 1984); Pachapa fine sandy clay and Gilat loam (Mualem 1976b); Poederlee loamy sand and Poederlee sand (Nemes et al. 2001); Cubbaroo clay loam and fine sand (Minasny and Field 2005); and Berlin sand (Peters 2013). These data sets of soils, with different textures and sources, were chosen because their hydraulic conductivity measurements covered both dry and intermediate wet ranges. Table 1 summarizes the measured properties of the soils used in this study.

Model features and parameters determination

The features of the proposed model and the effect of parameters (C_f, α, and β) on soil properties are addressed in this part. The relative hydraulic conductivity (k_r) – matric head (h) curve (RMC) with varying parameters is shown in Fig. 4. As seen from this figure, the slope of RMC within the capillary regime strongly depends on the fractal factor C_f, while the effect of C_f on the film flow is marginal. In other words, the pore size distribution of porous media controls the transport characteristic of capillary water but not adsorption film flow, which is consistent with the results found by Lu (2016). Additionally, it can be found that in the log-log scale, the relative hydraulic conductivity of capillary water increases as C_f increases with a given matric head. This is because the increase in C_f at a given range of pore sizes means an increase in the porosity (Khoshghalb et al. 2015), which strengthens the mass transfer capacity of porous media.

As shown in Fig. 4b, α controls the slope of RMC within the adsorption regime of the high matric head range. The

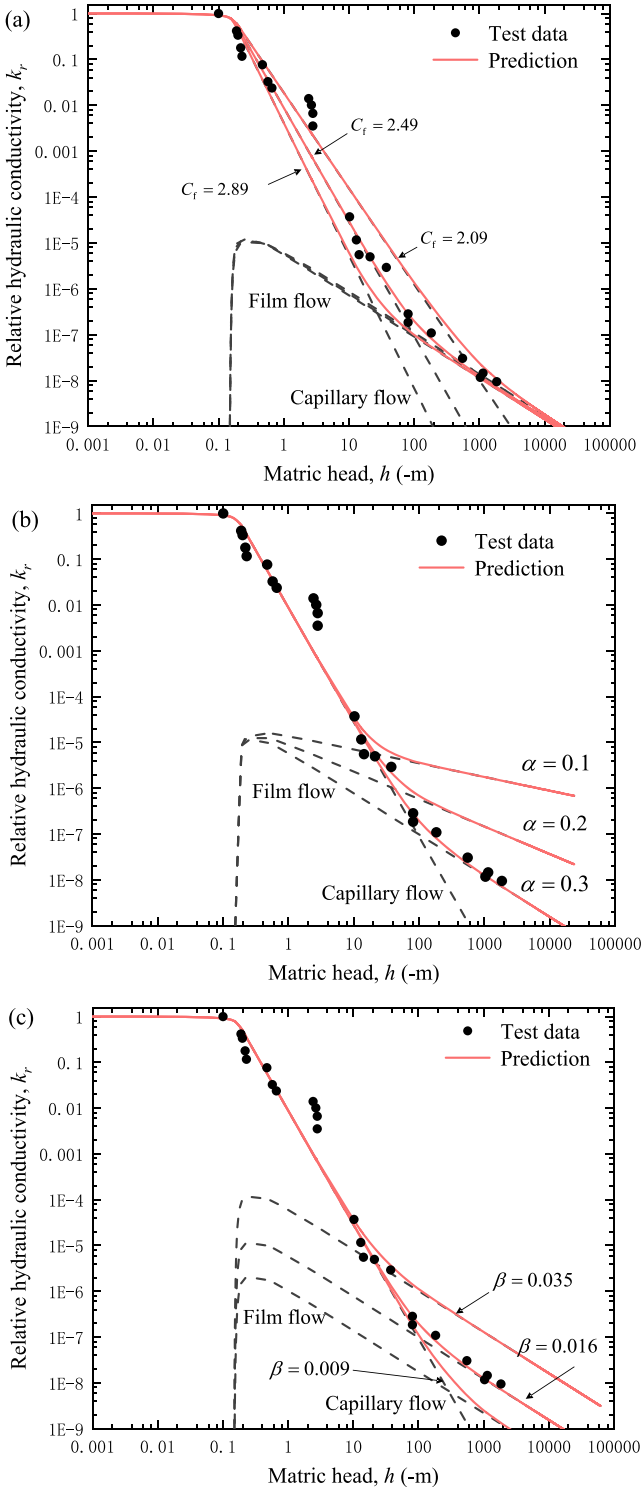

Fig. 4 Influences of parameters **a** C_f, **b** α, and **c** β on the relative hydraulic conductivity curve

physical mechanism may involve the adsorption strength of the material, which is controlled by mineral type (Lu 2016). For soils, experimental studies (Pachepsky et al. 1984; Mualem 1976b; Nemes et al. 2001; Minasny and Field 2005) have shown that the slope of RMC within the film-

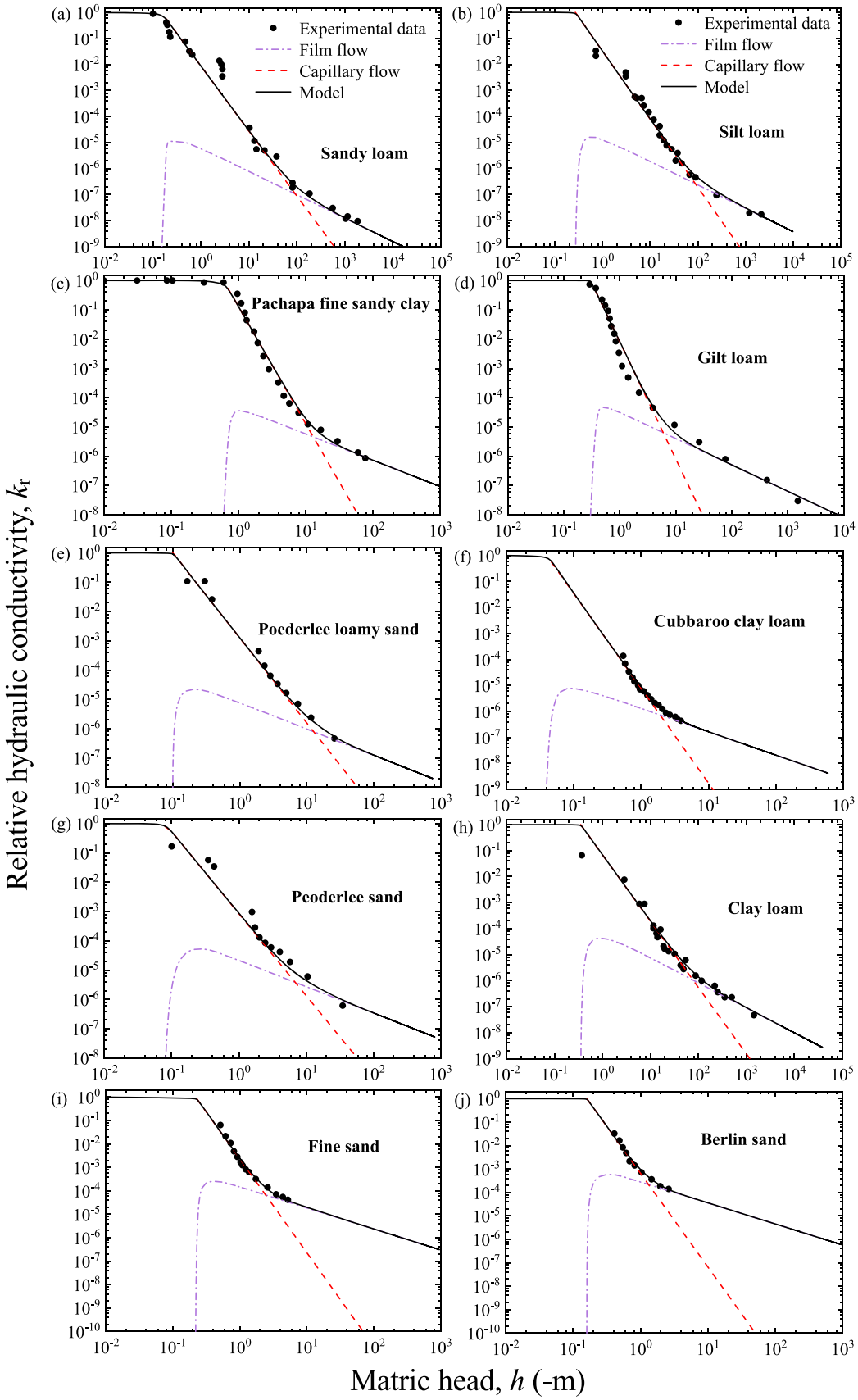

Fig. 5 **a**–**j** A comparison of the predicted relative hydraulic conductivity and experimental data

Table 2 Results of the fitted parameters for the relative hydraulic conductivity model

Data set	Reference	C_f	β	$h_{c,min}$ (–m)
Sandy loam	Pachepsky et al. (1984)	2.50	0.016	0.15
Silt loam	Pachepsky et al. (1984)	2.62	0.018	0.27
Clay loam	Pachepsky et al. (1984)	2.55	0.028	0.35
Pachapa fine sandy clay	Mualem (1976b)	3.90	0.022	0.60
Gilat loam	Mualem (1976b)	3.88	0.024	0.30
Poederlee loamy sand	Nemes et al. (2001)	2.90	0.020	0.10
Peoderlee sand	Nemes et al. (2001)	2.81	0.024	0.08
Cubbaroo clay loam	Minasny and Field (2005)	3.65	0.015	0.04
Fine sand	Minasny and Field (2005)	3.99	0.044	0.22
Berlin sand	Peters (2013)	3.93	0.062	0.16

dominated range in the log-log scale varies over a small range so that α can be approximated as a general constant to simplify the proposed model. In this paper, α is set to 0.3 and provides satisfactory agreement with test data.

From Fig. 4c, it can be seen that β governs the maximum relative hydraulic conductivity of the adsorbed water (corresponding to the maximum amount of adsorbed water) near the air-entry matric head, which may involve the specific area of a material. A larger β means that the soil has greater adsorption capacity, corresponding to a larger specific surface area and more hydrophilic mineral components.

It should be noted that, in the literature, model parameters of unsaturated hydraulic conductivity curves are commonly determined by fitting an equation to measured data, e.g., Yang and Mohanty (2015), Ghanbarian and Hunt (2017). It is well known that parameters may be coupled if there are more than two. This means that the optimal parameter combination obtained by the fitting is not unique (Yang and Mohanty, 2015). Only by narrowing the value range of each parameter as much as possible can we maintain the validity and uniqueness of the obtained parameters.

According to the preceding analysis of model features, it is known that the parameter coupling in the proposed model is very slight, which ensures the uniqueness of the optimal parameter combination. More specifically, the parameter C_f is controlled by the slope of RMC within the capillary regime; the parameter α is related to the slope of RMC within the adsorption regime of the high matric head range; and the parameter β can translate the RMC within the adsorption regime up and down to fit the measured data. Here, Sand Loam is taken as an example to give a general method for determining the parameters of the proposed model: (1) based on the overall characteristics of the measured data, the estimated ranges of C_f, α, and β can be determined as [2.20, 2.60], [0.25, 0.40], and [0.009, 0.020], respectively; (2) using the nonlinear least-square optimization method and the curve-fitting toolbox of MATLAB to determine C_f, α, and β values, i.e., C_f=2.49, α=0.3, and β=0.016.

Experimental validation

In this section, experimental data of various soils ranging from sand to loam are used to evaluate the proposed model. Figure 5 shows the comparison between the measured data and the proposed model, which is in good agreement with the various soils.

As seen in Fig. 5a, the proposed model agrees very well with the Sandy Loam data from the air entry value to a higher matric head of approximately 2,000 m. Due to the difference in the contribution of capillary flow and adsorptive film flow to water seepage, the RMC is divided into capillary- and adsorptive-dominated regions. For the Sandy Loam, the crossover point of RMC at a matric head is 100 m, which means that the adsorption-dominant region starts at this matric head and capillary flow dominates the lower matric head region. It is important to emphasize that the contribution of the adsorptive film flow is generally overlooked in the conventional hydraulic conductivity model so that the slope change phenomenon of the $k_r(h)$ test data cannot be explained. Figure 5b–j shows results similar to those of the sandy loam data set. The

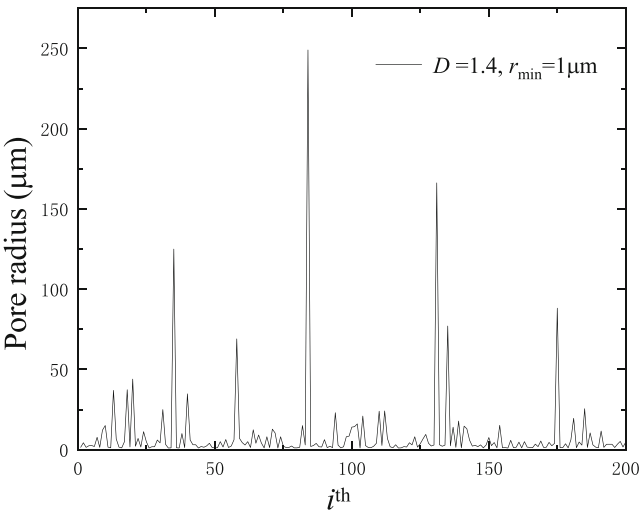

Fig. 6 Pore sizes simulated by the Monte Carlo method

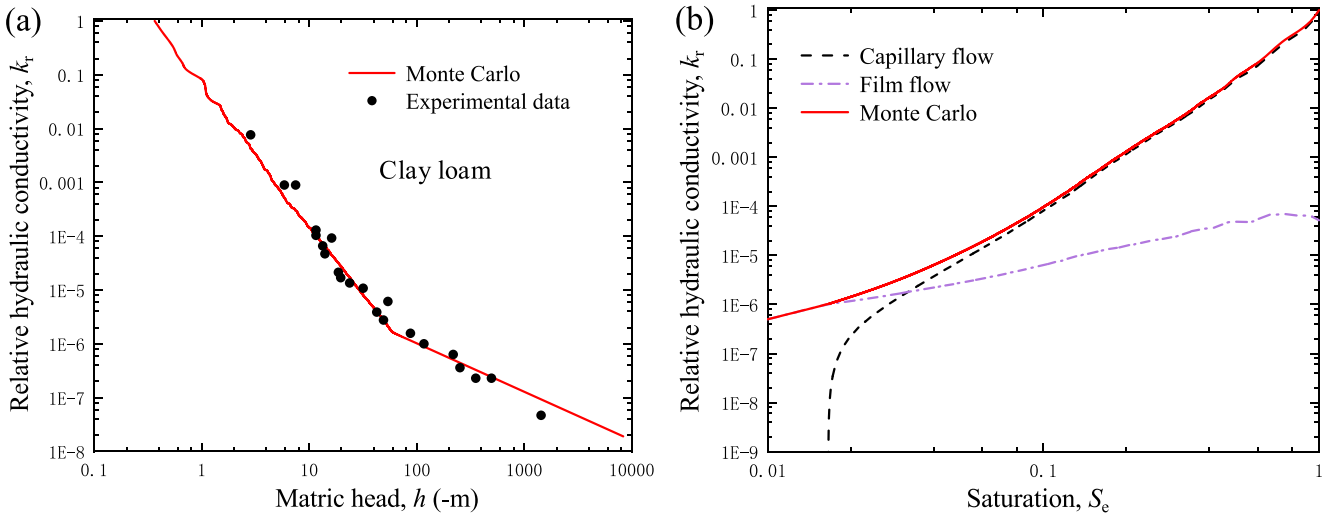

Fig. 7 Transport characteristics simulation of clay loam by the Monte Carlo method for **a** matric head and **b** saturation

model best-fit parameters of different soils are summarized in Table 2.

As a powerful and straightforward numerical technique, Monte Carlo simulation is employed here to further evaluate the proposed model. According to the fractal scaling law, pore size can be determined by a probability model of the Monte Carlo simulation (see Appendix A for the derivation):

$$r_i = \frac{r_{\min}}{(1-R_i)^{1/D_f}} \tag{34}$$

where R_i is an ith computer-generated random number with a range of 0–1. Figure 6 shows the pore size results for 200 Monte Carlo simulations. The pore size distribution result from the Monte Carlo simulation is discrete compared to the fractal analysis in section 'Specific model of relative hydraulic conductivity', and the dispersion implies that the predicted RMC is highly fluctuating.

Further, the Monte Carlo model of the relative hydraulic conductivity can be obtained (see Appendix A for the derivation):

$$k_r = \begin{cases} \left[\sum_{i=1(r_{\min})}^{j(r_c)} \frac{1}{(1-R_i)^{4/D_f}\tau_i} + \frac{8}{3}\sum_{i=j(r_c)}^{n(r_{\max})}\left(\frac{2\beta^3(1-R_c)^{-3\alpha/D_f}}{(1-R_i)^{(4-3\alpha)/D_f}\tau_i} - \frac{\beta^4(1-R_c)^{-4\alpha/D_f}}{(1-R_i)^{(4-4\alpha)/D_f}\tau_i}\right)\right] \Big/ \sum_{i=1(r_{\min})}^{n(r_{\max})} \frac{1}{(1-R_i)^{4/D_f}\tau_i} & , h \le h_{c,\min} \\ \left(\frac{16}{3}\beta^3\xi^{3\alpha}\sum_{i=1(r_{\min})}^{n(r_{\max})} \frac{1}{(1-R_i)^{(4-3\alpha)/D_f}\tau_i} - \frac{8}{3}\beta^4\xi^{4\alpha}\sum_{i=1(r_{\min})}^{n(r_{\max})} \frac{1}{(1-R_i)^{(4-4\alpha)/D_f}\tau_i}\right) \Big/ \sum_{i=1(r_{\min})}^{n(r_{\max})} \frac{1}{(1-R_i)^{4/D_f}\tau_i} & , h > h_{c,\min} \end{cases} \tag{35}$$

where R_c is a random number corresponding to the critical radius. $\xi = r^*/r_{\min}$ is a parameter indicating that the characteristic radius r^* is smaller than $r_{\min}$, subject to $\xi <= 1$.

Figures 7 and 8 illustrate the transport characteristics of Poederlee sand (Nemes et al. 2001) and clay loam (Pachepsky et al. 1984) captured by the proposed Monte Carlo model. As shown, the simulated RMC by the Monte Carlo method is in good agreement with the experimental data, capturing the transport behavior of water in a full range of matric head. For clay loam, an optimal combination of parameters can be found, i.e., D_f=1.45, α=0.3, and β=0.028, to make the model perform best. Based on these parameters, the relative hydraulic conductivity–saturation curve (RSC) is also presented in Fig. 7. It can be seen that the crossover point of the RSC of capillary flow and film flow is roughly at the position of $k_r = 2\times10^{-6}$, which implies that soil water transport is dominated by adsorption in the range where k_r is less than 2×10^{-6}, and the other range is dominated by capillarity. Additionally, for clay loam, the simulated maximum k_r of the film flow is approximately equal to 10^{-4}.

For Poederlee sand (see Fig. 8), D_f=1.22, α=0.3, and β=0.024 is an optimal combination of parameters. Compared to clay loam, the k_r is smaller than 10^{-6} at the position where the RSC of capillary flow and film flow intersect, and the simulated maximum k_r of the film flow of Poederlee sand is significantly smaller than 10^{-4}. This may be attributed to clay loam having a high fine particle content (corresponding to a large specific surface area) and hydrophilic minerals, which are beneficial to the retention and transport of film water. In contrast, Poederlee sand (with a higher proportion of large pores) has better transport capacity at lower matric heads dominated by capillarity.

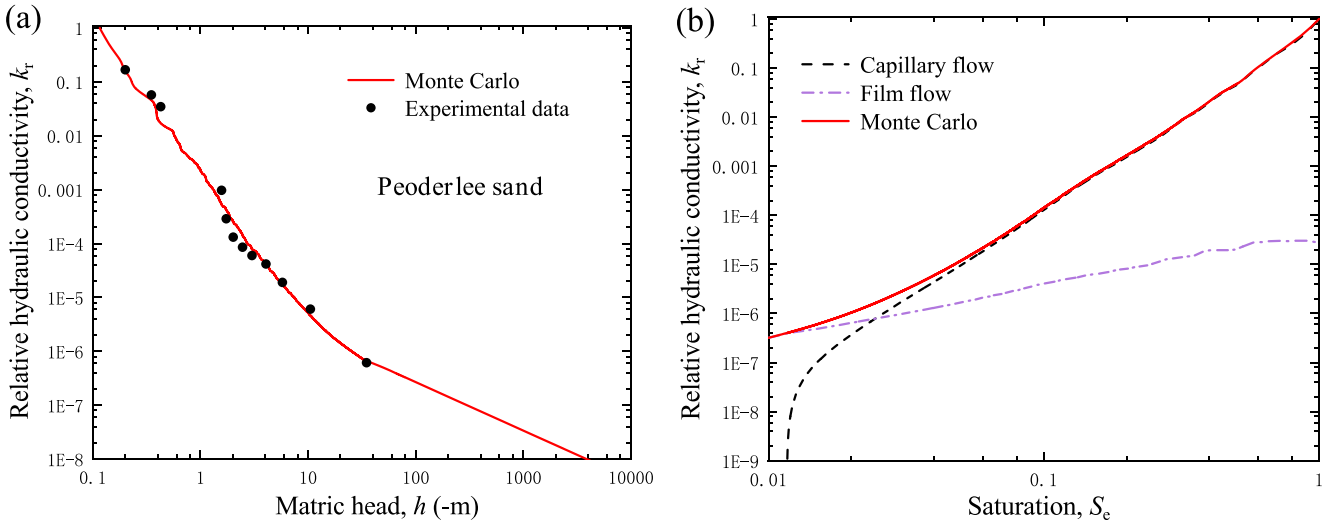

Fig. 8 Transport characteristics simulation of Poederlee sand by the Monte Carlo method for **a** matric head and **b** saturation

In summary, these examples indicate that the new physically based model, which uses a simplified configuration of pore water and the specific thickness concept of the adsorbed film, can well capture the transport behavior of water in the full range of the matric head.

Comparison and discussion

The previous section has verified that the model has a good prediction ability for experimental data. This section will further evaluate the superiority of the proposed model by comparing it with other models i.e., VG-B model (van Genuchten 1980) and K-M model (Lebeau and Konrad 2010). VG-B model and K-M model can be written as follows:

VG-B:

$$k_r(h) = \frac{1-(\alpha h)^{n-2}\left[1+(\alpha h)^n\right]^{-m}}{\left[1+(\alpha h)^n\right]^{2m}} \tag{36a}$$

where α, m, and n are the model parameters obtained by fitting measured data.

K-M:

$$k_r(h) = \left[\frac{1}{2}\mathrm{erfc}\left(\frac{\ln(h/h_m)}{\sqrt{2}\sigma}\right)\right]^{0.5}\cdot\left[\frac{1}{2}\mathrm{erfc}\left(\frac{\ln(h/h_m)}{\sqrt{2}\sigma}\right)+\frac{\sigma}{\sqrt{2}}\right]^2 \tag{36b}$$

where erfc() is the complementary error function, h_m is related to the matric head of the median pore radius, and σ is the standard deviation of the log-normal pore size distribution.

Table 3 Comparison of the mean squared error for the various models

Data set	MSE			Reference
	Proposed model	K-M model	VG-B model	
Sandy loam	1.13	18.3	4.36	Pachepsky et al. (1984)
Silt loam	0.27	11.3	1.72	Pachepsky et al. (1984)
Clay loam	0.50	5.44	0.78	Pachepsky et al. (1984)
Pachapa fine sandy clay	0.30	17.1	4.46	Mualem (1976b)
Gilat loam	0.54	33.8	24.67	Mualem (1976b)
Poederlee loamy sand	0.23	2.64	0.25	Nemes et al. (2001)
Peoderlee sand	0.54	6.99	0.67	Nemes et al. (2001)
Cubbaroo clay loam	0.04	1.05	0.14	Minasny and Field (2005)
Fine sand	0.08	0.48	0.84	Minasny and Field (2005)
Berlin sand	0.05	2.48	0.20	Peters (2013)

To clearly distinguish the differences in predictions of experimental data from different models, the mean squared error (which is an indicator of the overall magnitude of the residuals) is introduced here:

$$\mathrm{MSE} = \frac{1}{N}\sum_{i=1}^{N}\left[\ln\left(k_{r,i}^{\mathrm{meas.}}\right)-\ln\left(k_{r,i}^{\mathrm{pred.}}\right)\right] \quad (37)$$

where N is the number of the measured data, $k_{r,i}^{\mathrm{meas.}}$ and $k_{r,i}^{\mathrm{pred.}}$ Are the ith measured value and predicted value, respectively. Note that, in Eq. (37), the complete range of measured data can be well evaluated by log-transforming data.

Table 3 summarizes the MSE of the relative hydraulic conductivity predicted by each model (VG-B, K-M, and proposed models) for various porous media. As seen from Table 3, compared with the VG-B and K-M models, the proposed model performs best, occupying all of the smallest value of the MSE for each soil. Besides, the overall performance of these models can be reflected by the average value of MSE (aveMSE), which is 3.836 for the VG-M model, 9.958 for the K-M model and only 0.368 for the proposed model.

Additionally, the differences between these models can be clearly visualized as scatter plots of measured and predicted relative hydraulic conductivity values shown in Fig. 9. As shown, the VG-B and K-M models tend to generally underestimate the transport capacity of porous media, especially at low water saturations, which should be attributed to the fact that these two models ignored the contribution of film flow. In contrast, the predicted relative hydraulic conductivity values of the proposed fractal model are very close to the measured values, and these data sets show a much better linearship.

As can be seen, the proposed statistical-scale model represents an improvement of the capillary model, which provides a powerful explanation for the transport process of capillary and adsorbed water.

It should be noted that the extended model suffers from the limitations of an ideal capillary bundle that is assumed to be unconnected pores and a uniform pore cross-section. As a result, it cannot account for the effect of pore surface roughness and connectivity on water retention and the mass transfer of porous media such as nonlinear pressure drop and hysteresis. This problem can be partially overcome by providing specific roughness and connectivity to the pores. In this regard, some researchers have done a lot of interesting and progressive work, e.g., Chen et al. (2009), Ghanbarian et al. (2016), Ghanbarian and Hunt (2017). Especially, based on the percolation theory of porous media, Ghanbarian and Hunt (2017) established the hydraulic conductivity model over the entire range of water saturation with the fractal method. In this model, they quantified the effect of the interconnectivity of pores on the macroscopic fluid flow and considered the pore-

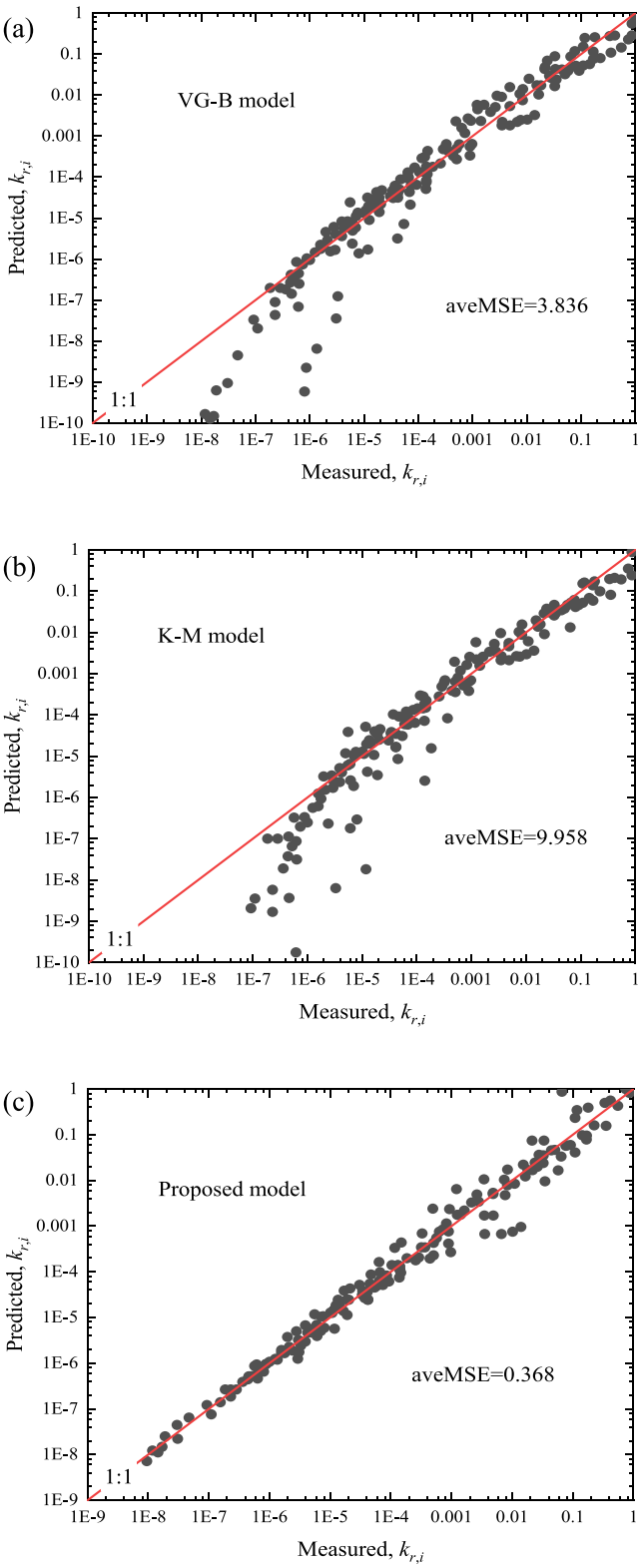

Fig. 9 Comparison of observed values and predicted values for the various models: **a** VG-B model, **b** K-M model, and **c** the proposed model

solid interface roughness effect, which improves the prediction effect of the model. It is clear that if a good pore image is available, it is certainly more realistic than a capillary bundle (Blunt et al. 2013).

On the other hand, to simplify the proposed model, this paper assumed that the water in the saturated pores is completely capillary water. This results in zero hydraulic conductivity of the adsorbed water in the case of saturation, which is not consistent with reality. However, in the wetting and medium wetting range, the adsorbed water content is much smaller than the capillary water, so the adsorbed water can be neglected. Additionally, this paper is more interested in the hydraulic conductivity of the adsorbed water in the dry range, and this simplification is acceptable. The proposed model can also be further enriched along these limitations.

Conclusions

A new and physically based transport model of unsaturated flow in porous media has been established in this paper, where the adsorbed water is taken into account to improve the prediction accuracy of relative hydraulic conductivity. In this study, the specific thickness of the adsorbed film was defined to describe the adsorption strength and adsorption capacity of porous media. The relative hydraulic conductivity model is derived on a statistical scale based on the Navier-Stokes equation and Darcy's law. Based on the model, the fractal-based relative hydraulic conductivity equation is also obtained, which captures the transport behavior of water in the full range of the matric head. The relative hydraulic conductivity predicted by the proposed model agrees well with the experimental data of various soils ranging from sand to loam.

Through parameter analysis, it can be found that (1) the pore size distribution has little effect on film transport, which is consistent with the discovery of Lu (2016); (2) parameters α and β involve the adsorption strength and adsorption capacity of materials, respectively. Finally, Monte Carlo simulation was used to prove the rationality of the proposed statistical model. The work in this paper is helpful to further understand and study the transport behavior of water in unsaturated soils, especially in the dry range.

Funding information This research did not receive any specific grant from funding agencies in the public, commercial, or not-for-profit sectors.

Appendix A: Monte Carlo simulation of fractal basis

According to the fractal scaling law, the total pore number from r_{min} to r_{max} can be determined by Eq. (26):

$$N_t = \left(\frac{r_{min}}{r_{max}}\right)^{-D_f} \tag{38}$$

Combining Eqs. (27) and (38), it can be obtained that

$$-\frac{dN(r)}{N_t} = D_f r_{min}^{D_f} r^{-D_f-1} dr = f(r)dr \tag{39}$$

where $f(r) = D_f r_{min}^{D_f} r^{-D_f-1}$ is defined as the probability density function (Yu et al. 2005; Xu et al. 2013). Additionally,

$$\int_{r_{min}}^{r_{max}} f(r)dr = 1-\left(\frac{r_{min}}{r_{max}}\right)^{D_f} \tag{40}$$

From the viewpoint of probability theory, $(r_{min}/r_{max})^{D}f = 0$ must be satisfied so that the probability density function $f(r)$ is meaningful. Fortunately, for natural porous media (e.g., soil), $r_{min}/r_{max} << 10^{-2}$. Hence, $(r_{min}/r_{max})^{D}f = 0$ holds approximately.

Then, the cumulative probability $R(r)$ of pores with size from r_{min} to r can be captured by integrating the probability density function $f(r)$ as follows:

$$R(r) = \int_{r_{min}}^{r} f(r)dr = 1-\left(\frac{r_{min}}{r}\right)^{D_f} \tag{41}$$

From Eq. (41), it is clear that R=0 as r=r_{min} and R=1 as r=r_{max}. Since the size of pores is randomly distributed in the range of r_{min} – r_{max} for natural porous media, R is a set of random numbers in the range of 0–1.

Rearranging Eq. (41) yields

$$r = \frac{r_{min}}{(1-R)^{1/D_f}} \tag{42}$$

Equation (42) indicates that the pore size in the range of r_{min}–r_{max} can be determined at a given random number R with a range of 0–1. Therefore, Eq. (42) can be seen as a Monte Carlo probability model capturing the pore size.

Combining Eqs. (25) and (42), the Monte Carlo model of relative hydraulic conductivity in the full range of the matric head can be obtained:

$$k_r = \begin{cases} \left[\sum_{i=1(r_{min})}^{j(r_c)} \frac{1}{(1-R_i)^{4/D_f}\tau_i} + \frac{8}{3}\sum_{i=j(r_c)}^{n(r_{max})}\left(\frac{2\beta^3(1-R_c)^{-3\alpha/D_f}}{(1-R_i)^{(4-3\alpha)/D_f}\tau_i} - \frac{\beta^4(1-R_c)^{-4\alpha/D_f}}{(1-R_i)^{(4-4\alpha)/D_f}\tau_i}\right)\right] \Big/ \sum_{i=1(r_{min})}^{n(r_{max})} \frac{1}{(1-R_i)^{4/D_f}\tau_i} & , h \le h_{c,min} \\ \left(\frac{16}{3}\beta^3\xi^{3\alpha}\sum_{i=1(r_{min})}^{n(r_{max})} \frac{1}{(1-R_i)^{(4-3\alpha)/D_f}\tau_i} - \frac{8}{3}\beta^4\xi^{4\alpha}\sum_{i=1(r_{min})}^{n(r_{max})} \frac{1}{(1-R_i)^{(4-4\alpha)/D_f}\tau_i}\right) \Big/ \sum_{i=1(r_{min})}^{n(r_{max})} \frac{1}{(1-R_i)^{4/D_f}\tau_i} & , h > h_{c,min} \end{cases} \tag{43}$$

where R_c is a random number corresponding to the critical radius. $\xi=r^*/r_{min}$ is a parameter indicating that the suction characteristic radius r^* is smaller than r_{min}, subject to $\xi<=1$.

Appendix B: notation

A_F	Cross-section area of film flow for a single pore (L^2)
A_F	Hamaker constant (ML^2T^{-2})
A_{REV}	Cross-section area of the REV (L^2)
C_f	Fractal factor
D_f	Area fractal dimension
D_T	Tortuosity fractal dimension
e	Electron charge (TI)
g	The gravity acceleration constant (LT^{-2})
h	Matric head (L)
$h_{c,max}$	Maximum matric head retained by capillarity (L)
$h_{c,min}$	Minimum matric head retained by capillarity (L)
k_B	Boltzmann constant ($ML^2T^{-2}\Theta^{-1}$)
k_r	Relative hydraulic conductivity
K_s	Saturated hydraulic conductivity (LT^{-1})
L_0	Representative length of a pore (L
L_t	Tortuous length of a pore (L)
n	Porosity
ΔP	Pressure drop ($ML^{-1}\ T^{-2}$)
$Q^C_{U,t}$	Total volumetric flow rate of capillary water (L^3T^{-1})
$Q^F_{U,t}$	Total volumetric flow rate of film flow (L^3T^{-1})
q^F	Volumetric flow rate of film flow for a single pore (L^3T^{-1})
$Q_{S,t}$	Total volumetric flow rate of saturated REV (L^3T^{-1})
$Q_{U,t}$	Total volumetric flow rate of unsaturated REV (L^3T^{-1})
r	Radius of grains or pores (L)
r^*	Suction characteristic radius (L)
r_c	Critical pore radius (L)
r_i	Radius of ith pore (L)
r_{max}	Maximum pore radius (L)
r_{min}	Minimum pore radius (L)
S	Surface area of the grain (L^2)
$S_{specific}$	Specific surface area of the grain (L^{-1})
T	Kelvin temperature (Θ)
V	Grain volume (L^3)
$\bar{v}_p$	Average liquid velocity (LT^{-1})
Z	Ion change
Π	Disjoining pressure ($ML^{-1}\ T^{-2}$)
Π_e	Ionic-electrostatic component of disjoining pressure ($ML^{-1}\ T^{-2}$)
Π_m	Molecular component of disjoining pressure ($ML^{-1}\ T^{-2}$)
Π_s	Structure component of disjoining pressure ($ML^{-1}\ T^{-2}$)
α	Adsorption strength of materials
β	Adsorption capacity of materials
δ	Specific thickness of adsorbed water
ε	Relative permittivity of water
ε_0	Permittivity of free space ($M^{-1}L^{-3}T^4I^2$)
λ	Shape factor
μ	Viscosity of pore water ($ML^{-1}\ T^{-1}$)
θ	Contact angle
θ_a	Adsorbed water film volume of a grain (L^3)
ρ	Density of pore water (ML^{-3})
σ	Water surface tension ($ML^{-1}\ T^{-2}$)
τ_i	Tortuosity of ith pore
τ	Pore tortuosity
ω	Film thickness (L)

References

Alexander L, Skaggs RW (1986) Predicting unsaturated hydraulic conductivity from the soil water characteristic. Trans Am Soc Agric Eng 29(1):176–184. https://doi.org/10.13031/2013.30123

Blunt MJ, Bijeljic B, Dong H, Gharbi O, Iglauer S, Mostaghimi P et al (2013) Pore-scale imaging and modelling. Adv Water Resour 51: 197–216. https://doi.org/10.1016/j.advwatres.2012.03.003

Bousfield DW, Karles G (2004) Penetration into three-dimensional complex porous structures. J Colloid Interface Sci 270(2):396–405. https://doi.org/10.1016/j.jcis.2003.10.017

Brooks RH, Corey AT (1964) Hydraulic properties of porous media. Hydrology papers 3. Colorado State University, Fort Collins, CO, 37 pp

Buckingham E (1907) Studies on the movement of soil moisture. Bulletin 38. US Gov Printing Office, Washington, DC

Burdine NT (1953) Relative permeability calculation size distribution data. Trans Am Inst Min Metall Pet Eng 198:71–78. https://doi.org/10.2118/225-g

Chen Y, Zhang C, Shi M, Peterson GP (2009) Role of surface roughness characterized by fractal geometry on laminar flow in microchannels. Phys Rev E 80(2):026301. https://doi.org/10.1103/PhysRevE.80.026301

Collis-George N (2010) A re-interpretation of the drainage moisture characteristic. Geoderma 189–190:87–90. https://doi.org/10.1016/j.geoderma.2012.05.008

Derjaguin BV, Churaev NV (1974) Structural component of disjoining pressure. J Colloid Interface Sci 49(2):249–255. https://doi.org/10.1016/0021-9797(74)90358-0

Derjaguin BV, Churaev NV, Muller VM (1987) Surface forces. Plenum, New York

Durner W, Fluhler H (2005) Soil hydraulic properties. In: Encyclopedia of hydrological sciences. Wiley, Hoboken, NJ

Ghanbarian B, Hunt AG (2017) Improving unsaturated hydraulic conductivity estimation in soils via percolation theory. Geoderma 303: 9–18. https://doi.org/10.1016/j.geoderma.2017.05.004

Ghanbarian B, Hunt AG, Daigle H (2016) Fluid flow in porous media with rough pore-solid interface. Water Resour Res 52(3):2045–2058. https://doi.org/10.1002/2015wr017857

Goss KU, Madliger M (2007) Estimation of water transport based on in situ measurements of relative humidity and temperature in a dry Tanzanian soil. Water Resour Res 43:W05433. https://doi.org/10.1029/2006WR005197

Guarracino L, Rötting T, Carrera J (2014) A fractal model to describe the evolution of multiphase flow properties during mineral dissolution. Adv Water Resour 67:78–86. https://doi.org/10.1016/j.advwatres.2014.02.011

Israelachvili JN (2011) Intermolecular and surface forces. Academic, San Diego

Jansik DP (2009) Flow processes in the dry regime: the effect on capillary barrier performance. MS Thesis, Oregon State Univ., Corvallis, OR, 69 pp

Khorshidi M, Lu N (2017) Intrinsic relation between soil water retention and cation exchange capacity. J Geotech Geoenviron Eng 143(4): 04016119. https://doi.org/10.1061/(asce)gt.1943-5606.0001633

Khoshghalb A, Pasha AY, Khalili N (2015) A fractal model for volume change dependency of the water retention curve. Géotechnique 65(2):141–146. https://doi.org/10.1680/geot.14.t.016

Kosugi K (1994) Three-parameter lognormal distribution model for soil water retention. Water Resour Res 30(4):891–901. https://doi.org/10.1029/93wr02931

Kosugi K (1996) Lognormal distribution model for unsaturated soil hydraulic properties. Water Resour Res 32:2697–2703. https://doi.org/10.1029/96WR01776

Langmuir I (1938) Repulsive forces between charged surfaces in water, and the cause of the Jones-ray effect. Science 88:430–432. https://doi.org/10.1126/science.88.2288.430

Lebeau M, Konrad JM (2010) A new capillary and thin film flow model for predicting the hydraulic conductivity of unsaturated porous media. Water Resour Res 46(12). https://doi.org/10.1029/2010wr009092

Lenormand R (1990) Liquids in porous media. J Phys Condens Matter 2: SA79–SA88

Lu N (2016) Generalized soil water retention equation for adsorption and capillarity. J Geotech Geoenviron Eng 142(10):04016051. https://doi.org/10.1061/(asce)gt.1943-5606.000152

Lu N, Zhang C (2019) Soil sorptive potential: concept, theory, and verification. J Geotech Geoenviron Eng 145(4):04019006. https://doi.org/10.1061/(asce)gt.1943-5606.0002025

McBride MB, Baveye P (1995) Mobility of anion spin probes in hectorite gels: viscosity of surficial water. Soil Sci Soc Am J 59(2):388. https://doi.org/10.2136/sssaj1995.03615995005900020017x

Minasny B, Field D (2005) Estimating soil hydraulic properties and their uncertainty: the use of stochastic simulation in the inverse modelling of the evaporation method. Geoderma 126(3–4):277–290. https://doi.org/10.1016/j.geoderma.2004.09.015

Mualem Y (1976) A new model for predicting the hydraulic conductivity of unsaturated porous media. Water Resour Res 12(3):513–521. https://doi.org/10.1029/wr012i003p00513

Mualem Y (1976b) A catalogue of the hydraulic properties of unsaturated soils. Technion, Israel Inst. of Technol., Haifa, Israel, 100 pp

Nemes A, Schaap MG, Leij FJ, Wösten JHM (2001) Description of the unsaturated soil hydraulic database UNSODA version 2.0. J Hydrol 251(3–4):151–162. https://doi.org/10.1016/S0022-1694(01)00465-6

Or D, Tuller M (2000) Flow in unsaturated fractured porous media: hydraulic conductivity of rough surfaces. Water Resour Res 36(5): 1165–1177. https://doi.org/10.1029/2000wr900020

Pachepsky YA, Shcherbakov RA, Varallyay G, Rajkai K (1984) On obtaining soil hydraulic conductivity curves from water retention curves (in Russian). Pochvovedenie 10:60–72

Peters A (2013) Simple consistent models for water retention and hydraulic conductivity in the complete moisture range. Water Resour Res 49(10):6765–6780. https://doi.org/10.1002/wrcr.20548

Peters A, Durner W (2008) A simple model for describing hydraulic conductivity in unsaturated porous media accounting for film and capillary flow. Water Resour Res 44(11). https://doi.org/10.1029/2008wr007136

Rudiyanto Sakai M, van Genuchten MT, Alazba AA, Setiawan BI, Minasny B (2015) A complete soil hydraulic model accounting for capillary and adsorptive water retention, capillary and film conductivity, and hysteresis. Water Resour Res 51(11):8757–8772. https://doi.org/10.1002/2015wr017703

Šimůnek J (2005) Models of water flow and solute transport in the unsaturated zone, chap 78. In: Encyclopedia of hydrological sciences. Wiley, Chichester, UK, pp 1171–1180

Tokunaga TK (2009) Hydraulic properties of adsorbed water films in unsaturated porous media. Water Resour Res 45(6). https://doi.org/10.1029/2009wr007734

Toledo P, Novy R, Davis H, Scriven L (1990) Hydraulic conductivity of porous media at low water content. Soil Sci Soc Am J 54:673–679. https://doi.org/10.2136/sssaj1990.03615995005400030060x

Tuller M, Or D (2001) Hydraulic conductivity of variably saturated porous media: film and corner flow in angular pore space. Water Resour Res 37(5):1257–1276. https://doi.org/10.1029/2000wr900328

Tuller M, Or D, Dudley LM (1999) Adsorption and capillary condensation in porous media: liquid retention and interfacial configurations in angular pores. Water Resour Res 35(7):1949–1964. https://doi.org/10.1029/1999wr900098

van Genuchten MT (1980) A closed-form equation for predicting the hydraulic conductivity of unsaturated soils. Soil Sci Soc Am J 44: 892–898. https://doi.org/10.2136/sssaj1980.03615995004400050002x

Xu C, Torres-Verdín C (2013) Pore system characterization and Petrophysical rock classification using a bimodal Gaussian density function. Math Geosci 45(6):753–771. https://doi.org/10.1007/s11004-013-9473-2

Xu P, Qiu S, Yu B, Jiang Z (2013) Prediction of relative permeability in unsaturated porous media with a fractal approach. Int J Heat Mass Transf 64:829–837. https://doi.org/10.1016/j.ijheatmasstransfer.2013.05.003

Yang Z, Mohanty BP (2015) Effective parameterizations of three nonwetting phase relative permeability models. Water Resour Res 51(8):6520–6531. https://doi.org/10.1002/2014WR016190

Yu B, Cheng P (2002) A fractal permeability model for bi-dispersed porous media. Int J Heat Mass Transf 45(14):2983–2993. https://doi.org/10.1016/s0017-9310(02)00014-5

Yu B, Zou M, Feng Y (2005) Permeability of fractal porous media by Monte Carlo simulations. Int J Heat Mass Transf 48(13):2787–2794. https://doi.org/10.1016/j.ijheatmasstransfer.2005.02.008

Zhang C, Lu N (2018) What is the range of soil water density? Critical reviews with a unified model. Rev Geophys 56(3):532–562. https://doi.org/10.1029/2018rg000597

Zhang ZF (2011) Soil water retention and relative permeability for conditions from oven-dry to full saturation. Vadose Zone J 10(4):1299. https://doi.org/10.2136/vzj2011.0019